Chapter 7.

IMAGE-FORMING ATOM-PROBE ANALYSIS.

7.1 The Effect of Imaging-Gas.

The data outlined above were taken, in the main, by field-evaporating the specimen in vacuum, and recording simultaneously and indiscriminately all types of ions formed. However, in conventional atom-probe analysis, image gas is almost always present during the analysis. This is for two reasons: first, so that the field-ion image may be inspected, to align features of interest with the probehole; second, the image gas generally lowers the field at which evaporation of metal atoms will occur (Nishikawa and Muller 1964). As the field is lower, the stress on the specimen is lower, and there is a reduced chance of the specimen failing; this may be particularly important, for example, in the study of specimens containing grain boundaries, where the purpose of the analysis is to study the segregation of embrittling impurities to the boundary.

No complete theoretical account of the evaporation-promotion mechanism exists, and therefore no convincing predictions can be easily made as to the effect of image-gas on the desorption pattern to be obtained when a metal is evaporated in the presence of such gas. It is therefore important to establish experimentally the correspondence between the spatial distribution of metal ions obtained by continuously field-evaporating a metal in vacuum, and the spatial distribution obtained by nanosecond-pulsed evaporation in the presence of an imaging gas. To do this, it is necessary to devise an experiment in which the desorbed metal ions will not be

obscured by the vastly greater number of field-ionized image-gas ions.

An elegant solution to this problem has been described by Panitz(1973, 1974) who has designed an atom-probe with a very short flight-path (100 mm). The detector is a chevron channel-plate with spherically-curved surfaces, so that all ions travel an equal distance between the specimen and the detector. Metal ions are nanosecond-pulse evaporated from the specimen, and then retarded to a final potential of 3 KV, to increase the length of the flight-time to the detector. The chevron channel-plate is switched on for a brief instant, using a high-voltage pulse, a preset delay after the initial evaporation pulse. Only ions with the correct mass-to-charge ratio to strike the detector during the duration of the second pulse will produce an output from the detector. A photograph of the output from the fibre-optic phosphor screen at the exit-side of the chevron plate will therefore show the spatial distribution of ions of a particular m/e ratio. As the chevron gating-pulse is extremely short there will be little interference from the random field-ionized gas current, at reasonable gas pressures ($<10^{-6}$ Torr). This instrument has been used to study the spatial distribution of W^{3+} and W^{4+} ions from a tungsten specimen (Panitz 1974); as the complex nature of the tungsten desorption image was not recognized, the conclusions reached will need considerable modification.

7.2 A Simple Imaging Atom-Probe.

A greatly-simplified version of the Panitz atom-probe was constructed for use in the present experimental work (fig(7.1)). The flight-distance between the specimen and the single flat 50 mm

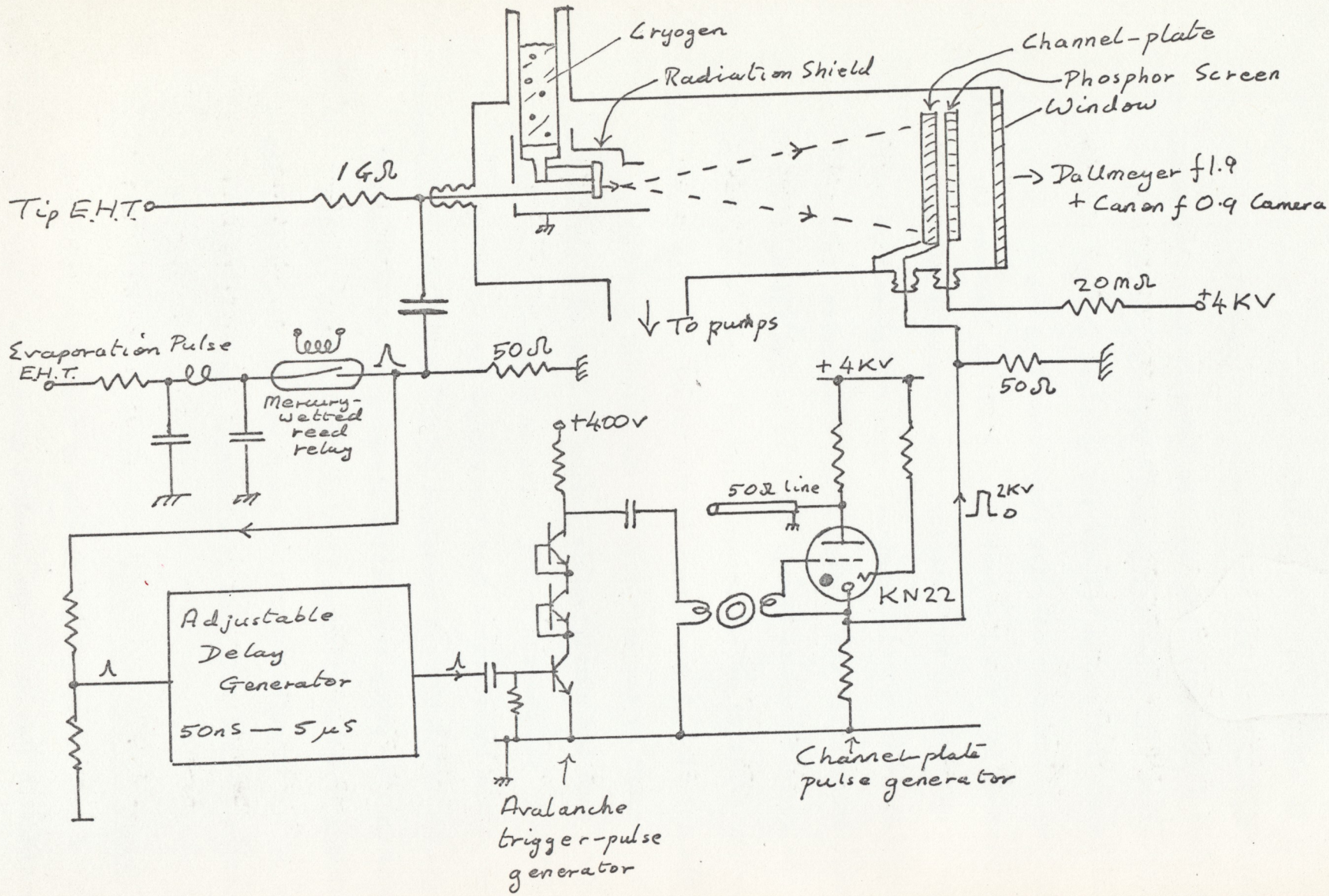

Fig 7.1 Schematic Diagram of Imaging Atom-Probe.

channel-plate used as a detector was short, so that a reasonable cone-angle of ions emitted from the specimen would be intercepted ($\simeq 20^{\circ}$). The short flight-path, ~120 mm, and the lack of any retarding or image-compressing lenses, restricted the mass resolution to be expected from the device. The path-lengths between the tip and the centre and edge of the detector are respectively 120 mm and 124 mm. The best possible mass resolution to be expected is given by

$$dm/m = -2\,dL/L \quad 1/15, \text{ or } dm \triangleq 4 \text{ at mass } 60.$$

The channel-plate used as detector was a Bendix 50 mm diameter x 40 um channel device, which was modified by evaporating a thin film of gold over the nichrome film which is supplied as the standard electrical contact to the channels. This was necessary (Panitz private communication) in order to allow the passage of large charging-currents during the gating-pulse. Assuming a 100 pF plate capacitance and a 5 nS risetime 2 KV pulse, the charging currents are of the order $Q/t = CV/t = 200$ amps., which would rapidly destroy the contact areas between the external electrodes and the resistive nichrome film.

The large 2 KV pulse used to gate the channel-plate was necessitated in part by the driving electronics, and partly by the non-linear gain-characteristics of the channel-plate (see below). The channel-plate gating pulse had to be produced a short variable time after the evaporation pulse, which is best derived from a jitter-free mercury-wetted reed relay (Regan 1973) which is asynchronous. An electronically-fired pulser using an EG & G KN 22 krytron as high-voltage switch was used to produce the gating pulse. It was found that there was a delay between initiating the output pulse and the actual output pulse; this delay was a minimum when

the krytron was operated at 4 KV, to produce a 2 KV output pulse. A simple TTL monostable circuit was used to vary the delay between the evaporation and the gating pulses. The minimum possible delay with the circuitry used was 350 nS, which restricted the minimum mass/charge ratio which was detectable to 30, at about 12 KV specimen voltage. The width of the gating pulse, which was governed by the length of the krytron charging line, was approximately 80 nS, with 5 nS rise and fall time. This pulse was made deliberately wide, although this limited the mass-resolution of the instrument, as it was found that the use of a short gating time (10 nS) caused problems in setting the delay, which is of course a function of specimen voltage. Using the short pulse it was easily possible to adjust the delay so that only the central area of the plate, or only the outer annulus, actually registered the arrival of a particular mass species. The overall jitter of the gating system was measured at less than 2 nS on a fast oscilloscope

No problems were found in operating the channel-plate at the extremely high voltage of 2 KV. Under DC conditions the noise level at such a voltage would be prohibitively high, but the observed number of noise pulses during the 80 nS gating time was extremely small. The output pulses produced much denser records on Tri-X film, with an apparently more uniform size of output pulse, than under DC conditions at 1500 volts, as in the experiments described above. This was probably due to ion feedback (Eschard and Manley 1971) in the straight channels of the channel-plate; electrons near the exit aperture of a channel ionize gas atoms or atoms adsorbed on the channel wall, and the positive ions thus formed return towards the input side of the plate under the influence of the electrostatic field in the channel. They may then collide with the channel wall

and initiate further electron avalanches; this process will continue until the surface of the channel becomes so charged that the channel gain is drastically reduced. The result will be a total output charge than the charge of the individual pulses. If the channel-plate is operated in the (relatively) high gas pressure of 10^{-5} Torr, then gas atoms ionized by the electrons will contribute significantly to the feedback process, while at lower pressures only adsorbed gases will contribute significantly. For ion feedback to occur it is necessary for the channel-plate voltage to be applied for a time which is longer than the time for an ion to travel the length of a channel. This will be, for an ion formed at the exit of the channel and accelerated down the whole length of if before hitting the wall, given by $t = (2\ m\ s^2/neV)$, where s is the channel length, m the ion's mass, ne its charge, and V the channel-plate voltage. For He_4^+ and s = 1,5 mm, V = 2 KV the flight-time is approximately 9 nanoseconds.

The output electron signal from the channel will therefore be augmented by ionic feedback events, at a high enough image gas pressure, if the gating pulse has a width of more than 9 nS for helium (or 35 nS for neon). Longer pulses, such as the 80 nS pulse used in these experiments, will give proportionately larger outputs until the channel becomes saturated. Equally, for operation in vacuum, the pulse gain at a given voltage will be smaller at small pulse-widths than the DC gain at the same voltage, by an amount which reflects the importance of ionic feedback from adsorbate atoms dislodged from the channel walls. These effects probably account for the observation by Panitz(1974) that a larger pulse voltage than expected had to be applied to his chevron channel-plate to record single ions; this was attributed

at the time to difficulty in transmitting the pulse to the plate. Electron transit times ($t \simeq 0{,}2$ nS) would be expected to cause a further drop in gain at sub-nanosecond pulsewidths, where the current-levels involved would probably be prohibitively large anyway.

In the experiments reported below the increased gain from gas-ionic feedback could be clearly seen. The output pulses from the phosphor were brighter when imaging-gas was present, and when the metal ions causing the scintillation were arriving near the beginning of the 80 nS gating pulse. With the 2 KV pulse-height there was no difficulty in recording the arrival of single ions even in vacuo with a 10 nS pulse-width. The different gain in vacuum and in imaging gas, while not of particular importance in this study, would be of importance in any attempt to use colour film to record different mass species in different colours, via a filter or two-colour phosphor, since fast colour films are sensitive to exposure levels.

For combined field-ion imaging and gated field-desorption atom-probe microscopy the single channel-plate detector appears to have significant advantages over the chevron plates used by Panitz. Although chevrons have nominally higher gain, they are delicate and expensive, and may only be operated at low image-gas pressures ($< 10^{-6}$ Torr). Muller has used a chevron as a single-particle detector in a conventional atom-probe (Muller and Tsong 1973) where the high gain of the chevron might be thought to be mandatory; he claims that the chevron does not produce afterpulses (which can be misinterpreted as metal/gas complex ions)in disagreement with Brenner and Mckinney (1972) who found significant numbers of afterpulses in a similar detector, in a careful comparison of the merits of different detectors. The present author has found that a photomultiplier external to

Fig. 7.2

Tungsten in the imaging atom-probe, 78°K; the specimen contains a grain boundary (arrowed)

a) Helium-ion image . b) All charge species; superimposed nanosecond evaporation pulses c) W^{3+} & WHe^{3+} in presence of helium image gas.

a)

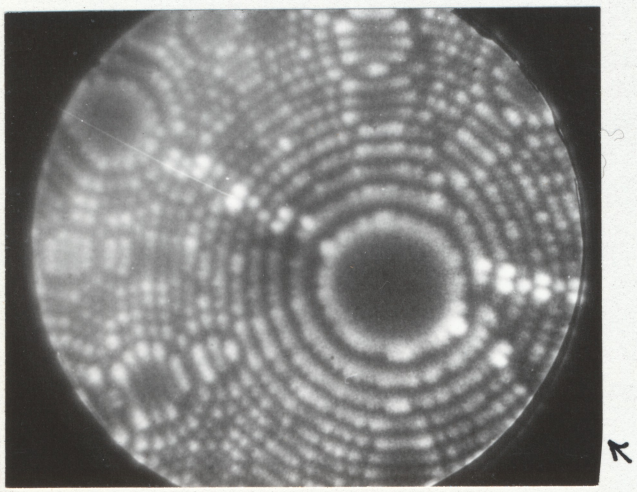

b)

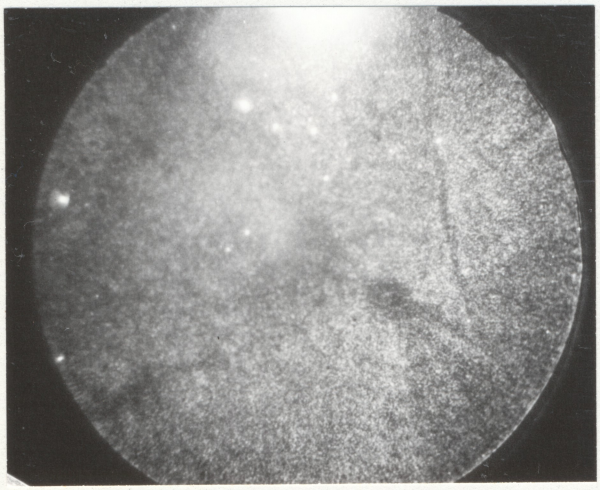

c)

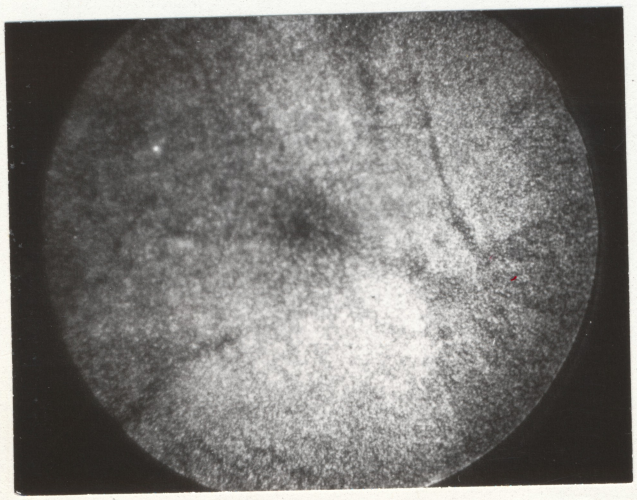

the vacuum sytem will easily detect the scintillations produced by a single ion on a single channel-plate; a fast phosphor (e.g. Levy-West YCS 70) produces adequate time-resolution for most purposes ($\simeq$ 15 nS) and operation of the plate at 1200 volts gives a satisfactory saturated output-pulse distribution; afterpulsing is also present for this type of detector. New types of single channel-plate now under development (Eschard etal 1974) which may be operated at very high voltages, to produce saturated after-pulse free gains of 10^8 or so, will apparently be even more suitable for single-ion detection in atom-probes and desorption microscopes than present channel-plates.

7.3 Results from the Imaging Atom-Probe.

As was mentioned at the beginning of this chapter, the imaging atom-probe was constructed in order to compare the field-desorption patterns obtained from nanosecond-pulsed evaporation in vacuum with those obtained in the presence of imaging-gas. The limited survey carried out with the atom-probe showed that, for tungsten and iridium at least, the major features of the patterns are obtained in both vacuum and image-gas. There are, however, some minor differences which are of interest.

7.3.1 Tungsten.

Some results from tungsten in vacuum and in helium are compared in Fig(7.2) ($78^{\circ}K$). Fig(7.2b) shows the typical pattern obtained by simultaneously recording all charge species produced by evaporating the specimen in vacuum (i.e. the channel-plate was run at 1450 volts DC while the specimen alone was pulsed).

Fig. 7.3

Tungsten in the imaging atom-probe, $20^{\circ}K$.

a) Helium image (low-angle boundary is arrowed)

b) W^{3+} & WHe^{3+} in the presence of helium image-gas.

a)

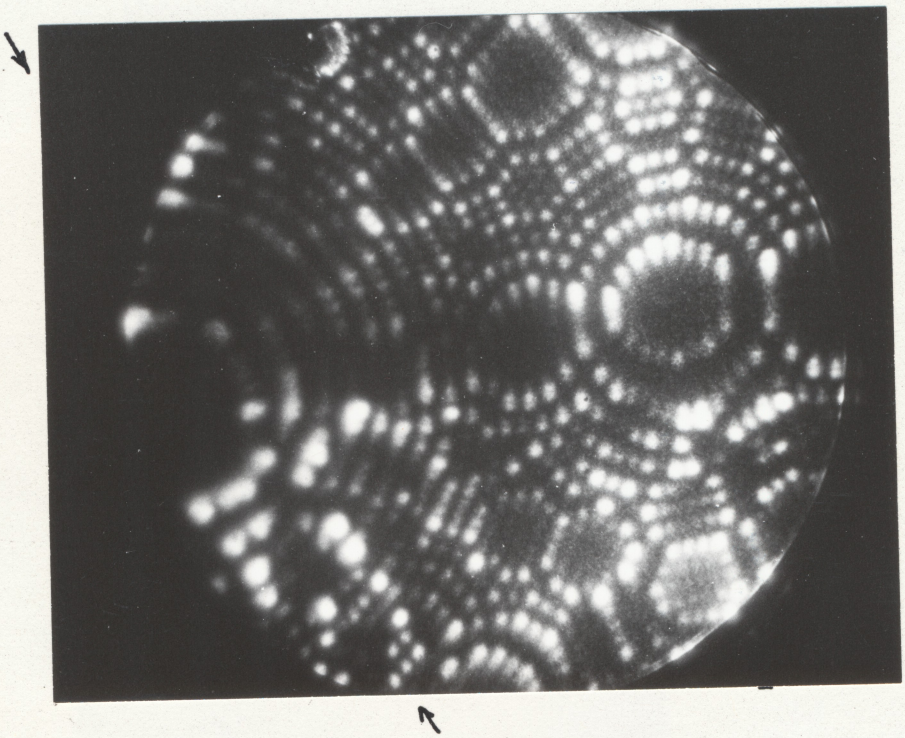

b)

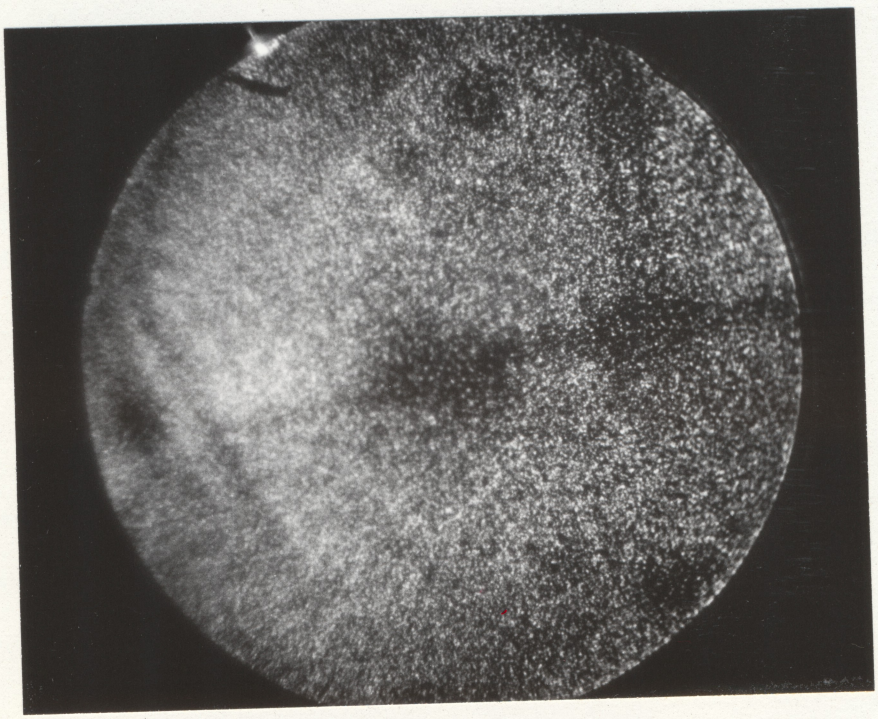

Fig(7.2c) shows the desorption pattern from the same specimen in the presence of helium, with only W^{3+} ions, or more probably WHe^{3+} ions(Muller 1969) being recorded. The pictures were obtained by superimposing many pulsed pictures, taking a time exposure of 5-20 seconds with the evaporation pulse generator running at approximately 20 Hz. The collapsing {110} rings could be clearly seen with the naked eye, and the presence (in helium) or absence (in vacuum) of a relatively bright centre to the (110) plane could be seen as the rings collapsed to the centre. Both vacuum and helium desorption images show the ring-structure around the (110) plane,which was described in Chapter 6, provided that sufficient numbers of {110} planes are evaporated to form the image. The zone decoration was somewhat more ragged in the WHe^{3+} desorption image than in the vacuum image; Turner (private communication) has found that W^{4+} is frequently obtained from the tungsten zone decoration in helium, and this may account for the observed faintness of the zone decoration in the WHe^{3+} image. The grain boundary which may be seen in the helium-ion image (7.2a) is seen clearly as a sharply-edged dark line in both of the desorption images.

The bright centre to the (110) plane in the 78°K W^{3+}/helium image is not seen at a much lower temperature, estimated as 10-20°K (fig(7.3)). This may be related to the lower abundance of WHe^{3+} at low temperatures, reported by Muller (1969), or to to formation of W^{4+} at the plane centre (Panitz 1974); equally, a reversion to the 78°K vacuum evaporation behaviour, where neither W^{3+} nor W^{4+} are observed at the plane centre, is a possibility at the higher low-temperature evaporation field.

A low-angle grain-boundary, which was barely discernable

in the helium image, is clearly seen in the W^{3+}/helium image as a relatively broad dark feature crossing the (110) pole. Other features of the image are similar to the vacuum/78°/nanosecond pulsed desorption image, as far as may be judged from the relatively 'noisy' pictures obtained.

The evaporation behaviour of the metal was found to be different in character to that which was observed at 78°K. At 78°K it is easy to set the evaporation rate so that the 110 rings shrink steadily and continuously. At the lower temperature the evaporation rate is found to be much more sensitive to the field: as the specimen standing voltage is raised, with the pulser running, little happens until suddenly the whole {110} ring system starts to evaporate, apparently from the centre outwards; 1 plane, or a small number of planes, evaporate in a fraction of a second, and the surface then becomes relatively stable again, with evaporation only taking place from a few high-index planes for the next few seconds; the {110} rings then evaporate again, and the whole cycle is repeated. The evaporation rate has been predicted to be particularly field-sensitive at low temperatures (Taylor 1970) but this cyclic type of evaporation behaviour makes the definition of the experimentally-observed evaporation-rate a matter of some debate.

7.3.2 Iridium.

A study of one of the f.c.c. metals in the imaging atom-probe was felt to be of particular interest, in view of the characteristic patterns shown by these metals during continuous vacuum evaporation. Iridium was chosen as a representative sample. Iridium has been studied previously in a conventional atom-probe by Brenner and McKinney (1968) who noted the formation of Ir^{2+}

Fig. 7.4

Iridium in the short atom-probe, 78°K:

a) Helium image b) Ir^{2+} in vacuum c) Ir^{3+} in vacuum.

a)

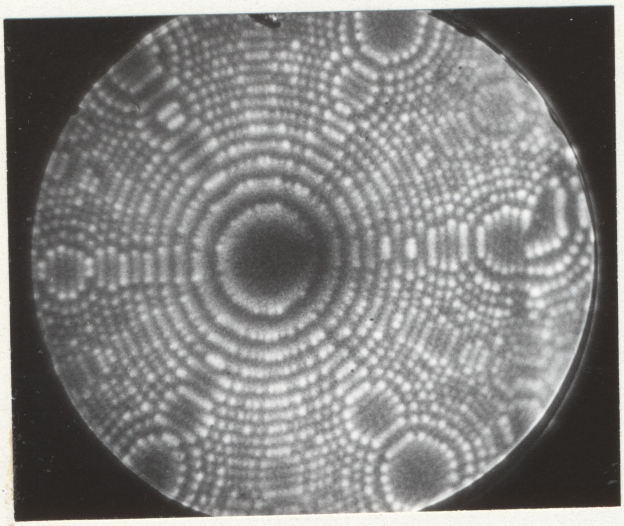

b)

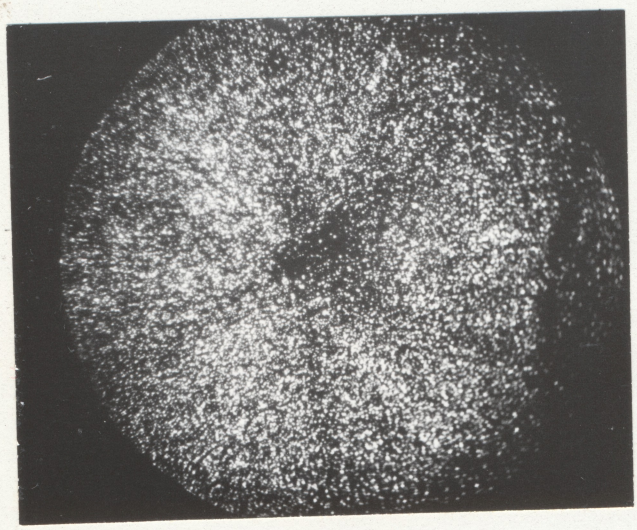

c)

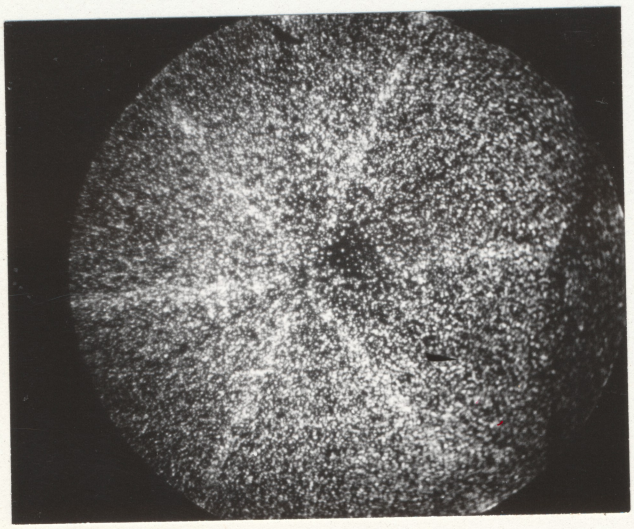

Fig 7.5

Iridium in the imaging atom-probe:

a) Helium-ion image b) Ir^{2+} or $IrHe^{2+}$ in the presence of helium c) Ir^{3+} or $IrHe^{3+}$ in the presence of helium.

a)

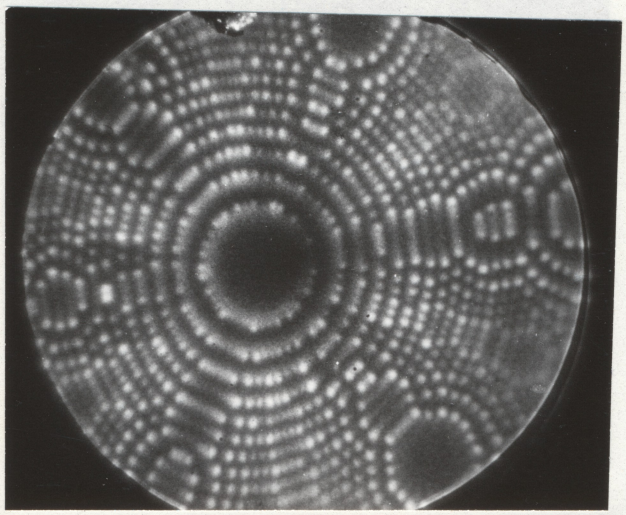

b)

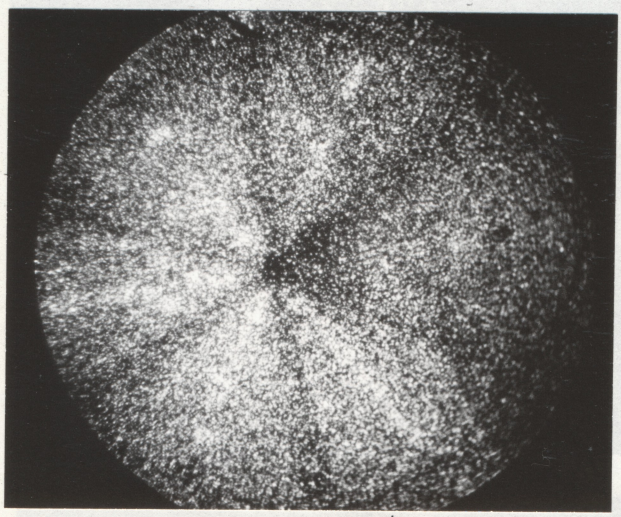

c)

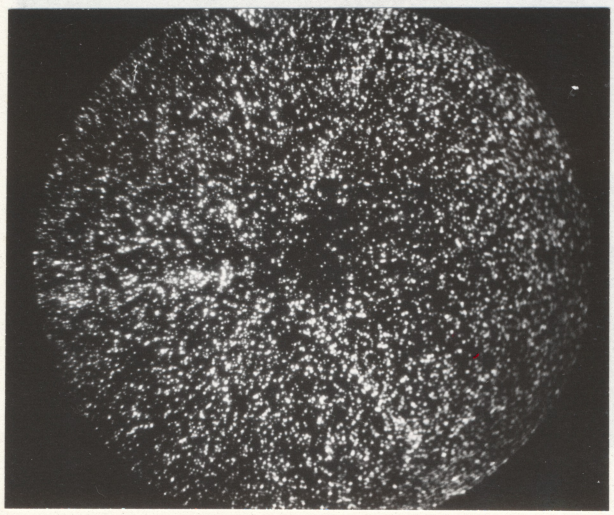

and Ir^{3+}, with the lower charge species predominating in helium, and the higher in vacuum. Muller(1969) has reported the formation of $IrHe^{2+}$ and $IrHe^{3+}$.

The results obtained in the present study are summarized in fig(7.4) and fig(7.5). Fig(7.4) shows the Ir^{2+} and Ir^{3+} images obtained in vacuum ($78^{o}K$), while fig(7.5) shows the same species (and helium complexes) in the presence of helium image-gas. The latter set were taken at a relatively fast evaporation rate, so that a reasonably large proportion of Ir^{3+} was obtained. The shift in abundance of the species between spectra taken in helium and vacuum, reported by Brenner and McKinney, was observed.

The micrographs obtained from Ir^{2+} and Ir^{3+} in vacuum and in helium all show the general characteristics of the iridium pulse-desorbed image (Chapter 6). They all contain alternate narrow bright and dark zone-lines radiating from (111) with pseudohexagonal symmetry, and a diffuse background. This eliminates the possibility that the bright zones are formed from one charge species and the background from the other. There are some specific differences in the character of the micrographs: the bright and dark zones are apparently broader in the Ir^{2+} images than in the Ir^{3+} images; the bright zone-lines are faint in the Ir^{2+}/vacuum images obtained; alternate bright zones in the Ir^{3+} image taken in helium are brighter or darker; Ir^{3+} ions are obtained from close to the centre of (111), while Ir^{2+} ions are not. These results are not entirely unexpected, as conventional atom-probe studies have occasionally indicated different ratios between the charge species obtained from different specimen areas

7.3.3 Cobalt-Tantalum.

The imaging atom-probe has a very high potential usefulness in the study of metallurgical problems. As has been emphasized above, the conventional small-probe-hole atom-probe has the disadvantage that a correlation between the position of the field-ion over the probe-hole, and the field-evaporated ions which pass through the probe-hole, has to be assumed. Correction for aiming errors may be made on a trial-and-error basis, but becomes impossibly difficult in the case of complex metallurgical specimens. If, for example, a grain boundary is being studied, with the object of studying the segregation of impurity atoms to the boundary, it is of interest to know whether any impurity atoms which are detected come actually from the boundary, or are present in the matrix on either side of, but close to, the boundary. As is seen in the results presented above, the grain boundary may show in a desorption image of the matrix ions as a dark or bright line, indicating significant deflections of the matrix ions at the boundary. This tells us nothing about the behaviour of any impurity atoms, which will differ from the matrix atoms in binding energy, polarizability, interaction with image-gas, etc. We conclude that a displacement of the probe-hole to a position at which matrix atoms from the position of the boundary are detected will not necessarily result in the detection of impurity atoms, or, if they are detected, will not yield accurate information on the source of the atoms. If instead of a probehole an imaging atom-probe is used, the appearance of a sharp line of segregant ions close to, but perhaps displaced from, the image of the boundary in the field-ion or matrix desorption images, immediately provides strong evidence that there are segregated impurity atoms at the boundary. Also, since now the

whole boundary is providing atoms for the analysis, only a few planes have to be evaporated from the specimen to provide the analysis, which will be of importance if the boundary moves through the specimen in an erratic manner, or if the specimen is much weakened by the presence of the boundary, as is often the case.

The same arguments apply with equal force to the analysis of small precipitates, especially when these have an evaporation field which is substantially different to that of the matrix, and hence protrude from or are recessed into the specimen surface. A cobalt-5% tantalum alloy was chosen to illustrate the use of the short atom-probe in a metallurgical context. Heat-treatment of this alloy by slowly cooling it from 800°C leads to the appearance of small precipitates in the field-ion image of the material, which have a higher evaporation field than that of the matrix. Analysis of the orientation and imaging properties of these precipitates led Hildon and coworkers (1973) to conclude that they were the Laves phase Co_2Ta in an f.c.c. cobalt matrix, and this composition has been confirmed by conventional atom-probe analysis (Turner private communication). It was found during the course of this analysis that the apparent composition of the precipitates was a function of the hydrogen concentration in the vacuum system and in the specimen itself. Atom-probe analysis in UHV following specimen outgassing at 200°C for a short while lead to the composition Co_2Ta, while analysis without such outgassing yielded a composition with a small and variable amount of cobalt and a large amount of tantalum; that is, cobalt was selectively removed from the precipitates by the action of the hydrogen.

A specimen of this alloy were procured and imaged in neon

Fig. 7.6

Desorption images from a cobalt/5% tantalum alloy, in the presence of neon image gas; 78°K.

a) Ta^{3+} b) Neon-ion image: the Laves-phase precipitates image brightly c) Co^{2+} image.

a)

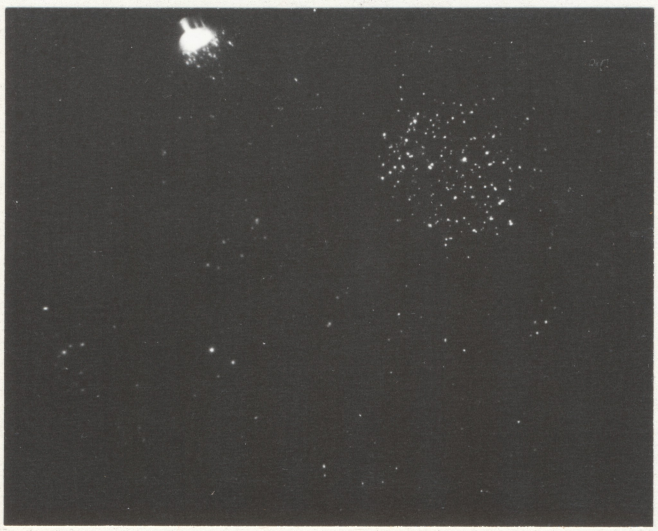

b)

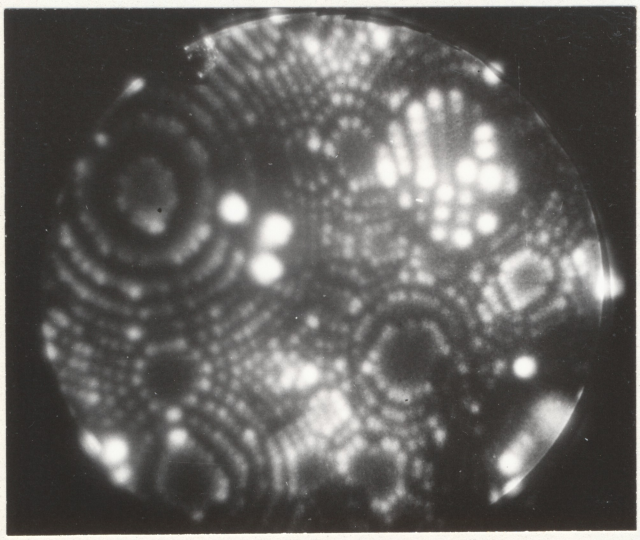

c)

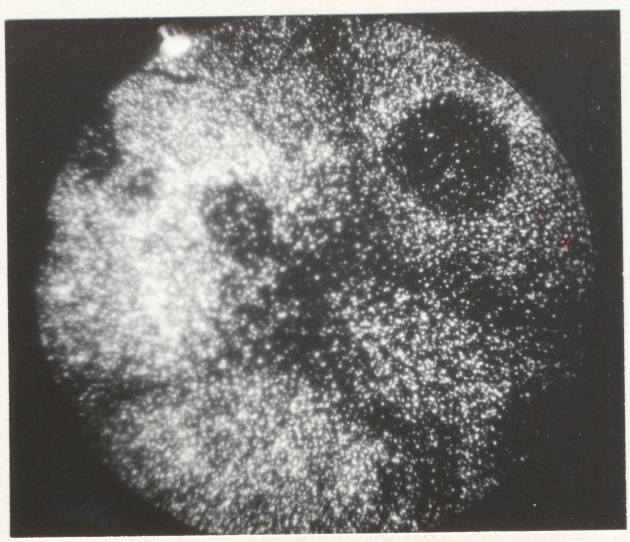

in the short atom-probe. Photographs were alternately taken of the neon field-ion image ($78^{o}K$) and of the desorption images formed by Co^{2+} (m/n = 29,45) and Ta^{3+}(m/n = 60,3) which conventional analysis had revealed as the majority charge species during evaporation in the presence of neon. A typical sequence is shown in fig(7.6). The precipitates are seen as bright irregular clusters, with some ring structure, in the neon-ion image (b). The tantalum-ion image (a) and the cobalt-ion image (c) show the position of the larger precipitates clearly as bright and dark regions respectively. The specimen had not been outgassed, and the background pressure was relatively high ($9\ 10^{-9}$Torr) so that some removal of cobalt from the precipitates was to be expected. Comparison of a series of such pictures showed that the tantalum ions arrived on the detector in an area closely corresponding to that expected from the size of the precipitate in the neon image, and conversely the edges of the precipitate corresponded with the boundary seen in the cobalt image. This experiment therefore shows that in this case at least conventional atom-probing would lead to sensible results, as there is no evidence for any severe divergence of the trajectories of the neon and the metal ions, and there is no evidence of any overlap of the desorption image of the precipitates and the adjacent area of the matrix.

7.4 Summary.

The construction of an imaging atom-probe, a simplified version of that described by Panitz, was outlined. The use of a single channel-plate driven by a fast high-voltage pulse as a time-resolved detector was described, and the occurrence and

effects of pressure-dependent afterpulsing in this detector were noted. The desorption images from iridium and tungsten in vacuum and in the presence of helium were compared. It was found that the images were similar in the two cases, but that there were some specific differences as well. It was shown that both of the common charge species from iridium showed the characteristic f.c.c. desorption-pattern. The desorption image of a grain boundary in tungsten was not greatly affected by the presence or absence of helium. Finally, an example of the use of the imaging-atom-probe in metallurgy was given; it was shown that a conventional atom-probe would not have been greatly affected by aiming-errors in this case.

Future work with imaging atom-probes will undoubtedly occur in the next few years. Areas of interest include atom-probe analysis of precipitates, segregation at grain boundaries, the formation of ordered alloys, the analysis of thin films, catalysis, field-adsorption and evaporation, to name but a few. Future instrumental developments will include the construction of more sophisticated instruments using new types of channel-plate with better gain and noise qualities, image-compressing lenses to enable a larger specimen area to be analysed at high resolution, and the development of data-handling techniques to extract compositional analysis and its spatial variation in the specimen from the photographs of the desorption image, or from the phosphor direct.